Superlattice Patterns in the Complex Ginzburg-Landau Equation with Multi-Resonant Forcing

Jessica M. Conway[1] and Hermann Riecke[1,2]

June 19, 2021

[1]Engineering Sciences and Applied Mathematics, Northwestern University, Evanston, IL 60208, USA

[2]Northwestern Institute on Complex Systems, Northwestern University, Evanston, IL 60208, USA

Abstract

Motivated by the rich variety of complex patterns observed on the surface of fluid layers that are vibrated at multiple frequencies, we investigate the effect of such resonant forcing on systems undergoing a Hopf bifurcation to spatially homogeneous oscillations. We use an extension of the complex Ginzburg-Landau equation that systematically captures weak forcing functions with a spectrum consisting of frequencies close to the 1:1-, the 1:2-, and the 1:3-resonance. By slowly modulating the amplitude of the 1:2-forcing component we render the bifurcation to subharmonic patterns supercritical despite the quadratic interaction introduced by the 1:3-forcing. Our weakly nonlinear analysis shows that quite generally the forcing function can be tuned such that resonant triad interactions with weakly damped modes stabilize subharmonic patterns comprised of four or five Fourier modes, which are similar to quasi-patterns with 4-fold and 5-fold rotational symmetry, respectively. Using direct simulations of the extended complex Ginzburg-Landau equation we confirm our weakly nonlinear analysis. In simulations domains of different complex patterns compete with each other on a slow time scale. As expected from energy arguments, with increasing strength of the triad interaction the more complex patterns eventually win out against the simpler patterns. We characterize these ordering dynamics using the spectral entropy of the patterns. For system parameters reported for experiments on the oscillatory Belousov-Zhabotinsky reaction we explicitly show that the forcing parameters can be tuned such that 4-mode patterns are the preferred patterns.

1 Introduction

Complex but ordered spatio-temporal patterns, characterized by multiple length scales, have been observed and studied in a range of systems. In particular in the Faraday system, in which a thin layer of fluid is vertically vibrated leading to patterns on the surface of the fluid, various kinds of superlattice patterns and quasi-patterns have been found experimentally depending on the frequency content of the forcing function [1–9]. Related complex patterns have also been observed in optical systems [10], in vertically vibrated fluid convection, where they arise from the competition of different instability mechanisms [11], and on the surface of ferrofluids driven by time-periodic magnetic fields, where they are due to spatial period-doubling [12].

From a purely spatial point of view the quasi-patterns as well as the superlattice patterns observed in the above forced dissipative systems are closely related to quasi-crystals obtained in thermodynamic equilibrium [13]. There the significance of damped, resonating modes for the stabilization of quasi-crystals has been recognized [14, 15]. Recently, two-dimensional quasi-crystals have been found in soft-matter systems [16]; their dodecagonal symmetry has been discussed in the context of

a Swift-Hohenberg-type model [17] that had previously been introduced to get insight into Faraday patterns [18].

The temporal aspect introduced by the forcing of non-equilibrium systems greatly increases the richness of patterns observed. To wit, contributing to the great variety of complex patterns observed in the Faraday system is the ability to control in detail the temporal wave form of the vibration's forcing function [3,5,7,19,20]. This allows extensive tuning of the interaction between plane waves of different orientation, which can in turn stabilize superlattice patterns and quasi-patterns. Two main stabilization mechanisms have been identified, both of which exploit the presence of weakly damped resonating modes. In one case the competition between plane-wave modes of different orientation is suppressed for a relatively narrow range in the angle subtended by the competing modes [19–22,53]. In the other case the self-coupling of each mode is strongly enhanced, rendering the competitive coupling between the modes effectively weak over a considerable range in the angle [22–28] and allowing patterns comprised of multiple modes to become stable [29]. The latter mechanism captures qualitatively the scenario envisioned for the stabilization of 'turbulent crystals' [15]. We will focus on this second mechanism and will make use of the fact that the temporal forcing introduces an additional symmetry that can be exploited to select or suppress certain types of patterns.

In this paper we investigate, motivated by the richness of patterns observed in the Faraday system, whether such complex spatio-temporal patterns are also accessible in systems undergoing a Hopf bifurcation to spatially homogeneous oscillations. These systems constitute a class that differs from those in which quasi-patterns have been observed previously and they may offer the potential for additional complexity through the interaction between the spontaneous oscillation arising from the Hopf bifurcation and the external forcing. Chemical oscillations like those observed in the Belousov-Zhabotinsky reaction are a classic example of such a system.

In the absence of any temporal forcing the Hopf bifurcations we have in mind lead to spatially homogeneous oscillations or long-wave traveling waves, which may break up to form spirals or more complex chaotic states (e.g. [30–34]). With temporal forcing, which in the case of the Belousov-Zhabotinsky reaction can be achieved by time-dependent illumination to exploit the photosensitivity of the reaction, the oscillations can become locked to the forcing and - depending on the ratio between the Hopf frequency and the forcing frequency - different types of patterns can arise [35–40]. Thus, forcing near twice the Hopf frequency can lead to competition between two types of domains differing in their temporal phase or to labyrinthine patterns. For a frequency ratio of 1:3, labyrinthine patterns, spirals, or competing domains have been observed. Ordered patterns with multiple length scales have been observed experimentally in chemical systems so far only when a *spatially periodic* illumination mask was applied to initialize the pattern [41, 42]. We focus on the case of *spatially uniform* illumination.

The organization of the paper is as follows. In Sec.2 we extend the complex Ginzburg-Landau equation (CGLE) to include the terms that describe the external forcing at various frequencies. The derivation of this equation for the Brusselator, which is a simple model for chemical oscillations, is sketched in the Appendix. In Sec.3 we present a linear stability analysis of the equation to find the onset of standing waves that are phase-locked to the driving. In particular we focus on the vicinity of the codimension-2 point at which the subharmonic and the harmonic standing waves bifurcate simultaneously. To determine the stability of the desired subharmonic patterns we derive in Sec.4 the corresponding amplitude equations by performing a weakly nonlinear analysis of the CGLE, and then use energy arguments to guide us in terms of the relative stability of various pattern comprised of different numbers of modes. In order to confirm our predictions for the pattern selection, we perform in Sec.5 numerical simulations of the CGLE in small and large domains, and characterize the temporal evolution of patterns by using a spectral pattern entropy. A brief account of these results has been published previously in [43].

2 The Complex Ginzburg-Landau Equation

We are interested in the formation of complex patterns in systems that undergo a Hopf bifurcation at vanishing wave number and that are forced at frequencies near integer multiples of the Hopf

frequency. Near the Hopf bifurcation and for weak forcing such systems can be described by a suitably extended complex Ginzburg-Landau equation (CGLE), the form of which can be derived using symmetry arguments.

In the absence of forcing the complex amplitude $A(t)$ satisfies the usual CGLE,

$$\frac{\partial A}{\partial t} = a_2 A + a_3 \Delta A + a_4 A|A|^2, \tag{1}$$

where $a_i \in \mathbb{C}, i = 1 \dots 4$ and Δ is the Laplacian in two dimensions [33]. The CGLE exhibits the normal-form symmetry $T_\tau : A \to Ae^{i\omega\tau}$ reflecting the invariance of the original system under translations of the time $\tilde{t}$ by an arbitrary amount τ, $T_\tau : \tilde{t} \to \tilde{t} + \tau$. Here ω is the Hopf frequency. The slow time t is given by $t = \delta^2 \tilde{t}$, $0 < \delta \ll 1$.

The extension of the CGLE that describes strongly resonant multi-frequency forcing of the form $F = f_1 e^{i\omega\tilde{t}} + f_2 e^{2i\omega\tilde{t}} + f_3 e^{3i\omega\tilde{t}} + c.c.$ can be obtained by considering the analogous center-manifold reduction of the extended dynamical system in which the forcing amplitudes f_1, f_2, and f_3 are considered as dynamical variables that vary on the slow time scale t. Under time translations T_τ they transform as $f_1 \to f_1 e^{i\omega\tau}$, $f_2 \to f_2 e^{2i\omega\tau}$, $f_3 \to f_3 e^{3i\omega\tau}$ (e.g. [44]). To cubic order in A the most general equation that is equivariant under T_τ is then given by

$$\frac{\partial A}{\partial t} = a_1 + a_2 A + a_3 \Delta A + a_4 A|A|^2 + a_5 \bar{A} + a_6 \bar{A}^2, \tag{2}$$

where $a_1 = b_{11} f_1 + b_{12} \bar{f}_2 f_3$, $a_2 = b_{21} + b_{22}|f_3|^2$, $a_5 = b_{51} f_2$, $a_6 = b_{61} f_3$. The b_{ij} are O(1) complex coefficients. For all terms to appear at the same order in the final amplitude equations, we use the scaling $A(t) = O(\delta)$, $f_1 = O(\delta^3)$, $f_2 = O(\delta^2)$, and $f_3 = O(\delta)$. Spatial coordinates are scaled as $(x, y) = \delta(\tilde{x}, \tilde{y})$, where $(\tilde{x}, \tilde{y})$ are the original spatial coordinates of the system.

The forcing terms f_j satisfy decoupled evolution equations on their own. In the simplest case this evolution expresses a detuning ν_j of the forcing f_j from the respective resonance and the f_j satisfy

$$\frac{df_j}{dt} = i\nu_j f_j, \qquad j = 1 \dots 3. \tag{3}$$

In general, the detuning introduces time dependence into (2).

In a previous study [45] we investigated the simpler case in which the forcing parameter f_1 satisfies $b_{11} f_1 = -b_{12} \bar{f}_2 f_3$ and the detuning parameter ν_3 satisfies $\nu_3 = 3\nu_2/2$, which allowed us to make all coefficients of the extended CGLE (2) time-independent by a transformation $A \to Ae^{i\nu_2 t/2}$. For that case we found that the possibly stable superhexagon pattern, a superlattice pattern, arises in a transcritical bifurcation. We showed that the amplitudes on the upper branch of the transcritical bifurcation are $O(1)$ and that therefore a weakly nonlinear analysis taken to cubic order is insufficient to describe these patterns. The bifurcation is transcritical because the quadratic term in the CGLE introduces also a quadratic term in the amplitude equations describing the competing Fourier modes. To eliminate the latter quadratic term without losing the resonant triad interaction we choose in the following the forcing near twice the Hopf frequency to be quasi-periodic,

$$f_2 = f_{21} + f_{22} \qquad \text{with} \qquad \frac{df_{21}}{dt} = i\nu_{21} f_{21}, \quad \frac{df_{22}}{dt} = i\nu_{22} f_{22}. \tag{4}$$

The difference between the two detunings ν_{21} and ν_{22} introduces then a periodic time dependence in (2). To obtain the desired patterns, we exploit the spatiotemporal resonances induced by the time dependence and focus on patterns that are subharmonic in time. The quadratic interaction of two subharmonic modes induces a harmonic mode and does not generate a quadratic term in the amplitude equation for the subharmonic mode. Consequently, we expect a pitch-fork bifurcation.

Considering the quasi-periodic forcing (4) we simplify (2) by absorbing the time dependence of f_{21}, $e^{i\nu_{21}t}$, into A through the transformation $A \to Ae^{i\nu_{21}t/2}$. Further, we write $a_3 = 1 + i\beta$ by rescaling the spatial coordinates and $a_4 = -(1 + i\alpha)$ by rescaling A. We focus on the case of a supercritical Hopf bifurcation and choose the real part of a_4 to be negative. We now introduce restrictions on the forcing f_j for the purpose of making the analysis manageable at the expense of

some generality. To eliminate the homogeneous term a_1 we choose $b_{11}f_1 = -b_{12}(\bar{f}_{21} + \bar{f}_{22})f_3$. To remove the time dependence from the $\bar{A}^2$ term we choose $\nu_3 = 3\nu_{21}/2$. This yields

$$\frac{\partial A}{\partial t} = (\mu + i\sigma)A + (1 + i\beta)\Delta A - (1 + i\alpha)A|A|^2 + (\gamma_1 + \gamma_2 e^{i(\nu_{22}-\nu_{21})t})\bar{A} + \eta\bar{A}^2. \tag{5}$$

Here the growth rate μ is modified by the forcing function $|f_3|^2$, σ is a linear function of the detuning ν_{21}, and η is a complex linear function of $|f_3|$. We rewrite η in magnitude and phase, $\eta = \rho e^{i\Phi}$, and write $\gamma_1 = \gamma\cos(\chi)$ and $\gamma_2 = \gamma\sin(\chi)$ with χ characterizing the relative forcing strengths. Finally we set $\nu \equiv \nu_{22} - \nu_{21}$, to get the version of the complex Ginzburg-Landau equation (CGLE) that we will investigate in the following,

$$\frac{\partial A}{\partial t} = (\mu + i\sigma)A + (1 + i\beta)\Delta A - (1 + i\alpha)A|A|^2 + \gamma\left(\cos(\chi) + \sin(\chi)e^{i\nu t}\right)\bar{A} + \rho e^{i\Phi}\bar{A}^2. \tag{6}$$

In this paper we stay below the Hopf bifurcation and focus on the case $\mu < 0$. As in the Faraday system, in the absence of forcing, the only solution is then the basic state $A = 0$.

3 Linear Stability Analysis

To obtain the onset of standing waves that are phase-locked to the driving we consider the stability of the solution $A = 0$ of (6) [36]. Linearizing (6) about $A = 0$ and splitting the equations into real and imaginary parts by setting $A = A_r + iA_i$, we obtain linear partial differential equations for A_r and A_i. Since these equations are time-periodic with period $2\pi/\nu$ we use Floquet theory in the same way as described in [46]. The solutions to the linear problem in Floquet form are

$$\begin{pmatrix} A_r \\ A_i \end{pmatrix} = e^{(\hat{\delta}+i\zeta)\nu t} \sum_{n=-\infty}^{\infty} \begin{pmatrix} X_n \\ Y_n \end{pmatrix} e^{in\nu t + ikx} + c.c. \tag{7}$$

Here $e^{(\hat{\delta}+i\zeta)t}$ is the Floquet multiplier. We restrict ζ to two values corresponding to a harmonic response ($\zeta = 0$) or to a subharmonic response ($\zeta = 1/2$). To obtain the neutral curve for the standing waves, the ansatz (7) is substituted into the linearized system with $\hat{\delta} = 0$, yielding the infinite-dimensional system of equations

$$\sum_{n=-\infty}^{\infty} e^{i(n+\zeta)\nu t}\left\{\begin{pmatrix} \mu - k^2 + \gamma(k)\cos(\chi) - i(n+\zeta)\nu & -\sigma + \beta k^2 \\ \sigma - \beta k^2 & \mu - k^2 - \gamma(k)\cos(\chi) - i(n+\zeta)\nu \end{pmatrix}\begin{pmatrix} X_n \\ Y_n \end{pmatrix}\right. \tag{8}$$

$$\left. + \frac{\gamma(k)\sin(\chi)}{2}\left[\begin{pmatrix} 1 & i \\ i & 1 \end{pmatrix}\begin{pmatrix} X_{n+1} \\ Y_{n+1} \end{pmatrix} + \begin{pmatrix} 1 & -i \\ -i & 1 \end{pmatrix}\begin{pmatrix} X_{n-1} \\ Y_{n-1} \end{pmatrix}\right]\right\} = 0,$$

which can be written as a matrix equation:

$$\mathbf{M}(\zeta)\mathbf{v} = \gamma(k)\mathbf{L}\mathbf{v}, \tag{9}$$

where

$$\mathbf{v} = (... \; X_{n-1} \; Y_{n-1} \; X_n \; Y_n \; X_{n+1} \; Y_{n+1} \; ...)^T.$$

Here $\mathbf{M}$ is block-diagonal and $\mathbf{L}$ couples adjacent modes (X_n, Y_n) and $(X_{n\pm1}, Y_{n\pm1})$. Equation (9) is a generalized eigenvalue problem for the eigenvalue $\gamma(k)$, which represents the forcing amplitude at the onset of the instability for a given k. In our formulation of the linear problem γ is assumed to be real; complex eigenvalues therefore do not correspond to solutions of the original problem. To solve for the eigenvalues for a given value of the wave number k, we truncate the sum in (9) at some N and calculate the eigenvalues. We test for convergence by requiring that for the real eigenvalues $\gamma_i^{(N)}$ the total change in all eigenvalues when N is increased by 1 is smaller than a tolerance Δ,

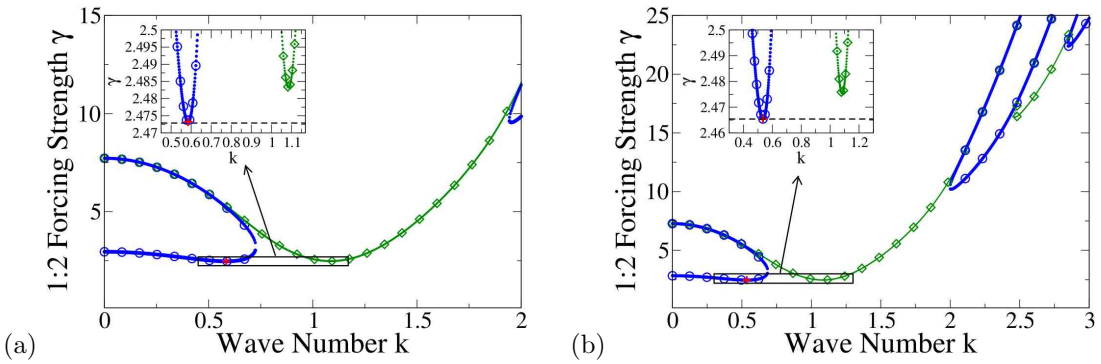

Figure 1: Harmonic (green, diamonds) and subharmonic (blue, circles) neutral stability curves for $\mu = -1$, $\sigma = 4$, $\beta = 3$. The parameters χ and ν are tuned to obtain the desired K. (a) For $K = 1.857$, $\chi = 0.4883189$ and $\nu = 3.824884$. (b) For $K = 2$, $\chi = 0.4767180$ and $\nu = 4.2$.

$\sum(\gamma_i^{(N+1)} - \gamma_i^{(N)})^2 \leq \Delta = 10^{-10}$. We find that generally $N = 10$ is sufficient. Repeating this process over a range of k we construct the neutral stability curves $\gamma^{(H)}(k)$ for the harmonic mode ($\zeta = 0$) and $\gamma^{(S)}(k)$ for the subharmonic mode ($\zeta = 1/2$). The global minimum of these curves yields the respective critical values $(k_c^{(H)}, \gamma_c^{(H)})$ and $(k_c^{(S)}, \gamma_c^{(S)})$.

The weakly nonlinear analysis below shows that weakly damped harmonic modes have a strong impact on the selection of subharmonic patterns via resonant triad interactions. Our aim is to exploit this sensitivity to stabilize complex patterns like superlattice patterns. We therefore focus here on parameters for which the minimum of the harmonic mode is only slightly above that of the subharmonic mode; we use $\gamma_c^{(H)} - \gamma_c^{(S)} = 0.01$. The resonant triads rely on spatiotemporal resonances that depend decisively on the wavenumber ratio $K \equiv k_c^{(H)}/k_c^{(S)}$. We consider the two cases $K = 2\cos(\tan^{-1}(2/5)) = 1.857$ and $K = 2$ and show in Fig.1 the corresponding neutral stability curves for $\gamma_c^{(H)} - \gamma_c^{(S)} = 0.01$.

Varying the parameter χ characterizing the ratio of forcing strengths near the 1:2-resonance shifts the critical forcing parameters $\gamma_c^{(H)}$ and $\gamma_c^{(S)}$ relative to each other, while varying the parameter ν characterizing the detuning difference shifts the critical wavenumbers $k_c^{(H)}$ and $k_c^{(S)}$. Requiring $\gamma_c^{(H)} - \gamma_0^{(S)} = 0.01$ for a fixed value of K defines a codimension-2 point that determines both χ and ν. For fixed $K = 2$ their dependence on the dispersion β and the damping μ is illustrated in Fig.2 along with the corresponding values of $\gamma_c^{(S)}$ and $k_c^{(S)}$. Since $\bar{A}$ satisfies the CGLE with the opposite signs of the imaginary parts of the equation, only positive values of β need to be considered.

For $\chi = 0$ the critical wave number is given by $k_c^2 = (\mu + \nu\beta)/(1 + \beta^2)$ corresponding to a critical forcing $\gamma_c^2 = (\nu - \mu\beta)^2/(1 + \beta^2)$ [36]. Thus, k_c has a local maximum and $k_c^2 \sim 1/\beta$ for large β; qualitatively the same behaviour is found at the codimension-2 point, as illustrated in Fig.2d. Fig.2c confirms that the amount of forcing necessary to generate patterns increases as one goes further below the Hopf bifurcation, i.e. as μ becomes more negative.

4 Weakly Nonlinear Analysis

To determine the stability of the desired subharmonic patterns we derive the corresponding amplitude equations by performing a weakly nonlinear analysis of (6). We then use energy arguments to guide us in terms of the relative stability of the various pattern comprised of different numbers of modes. We are in particular interested in the stability of patterns comprising three or more modes.

4.1 Amplitude Equations

Splitting the CGLE (6) again into real and imaginary parts, we obtain a system of real partial differential equations. For a subharmonic pattern with N modes, we expand (A_r, A_i) about $(0, 0)$

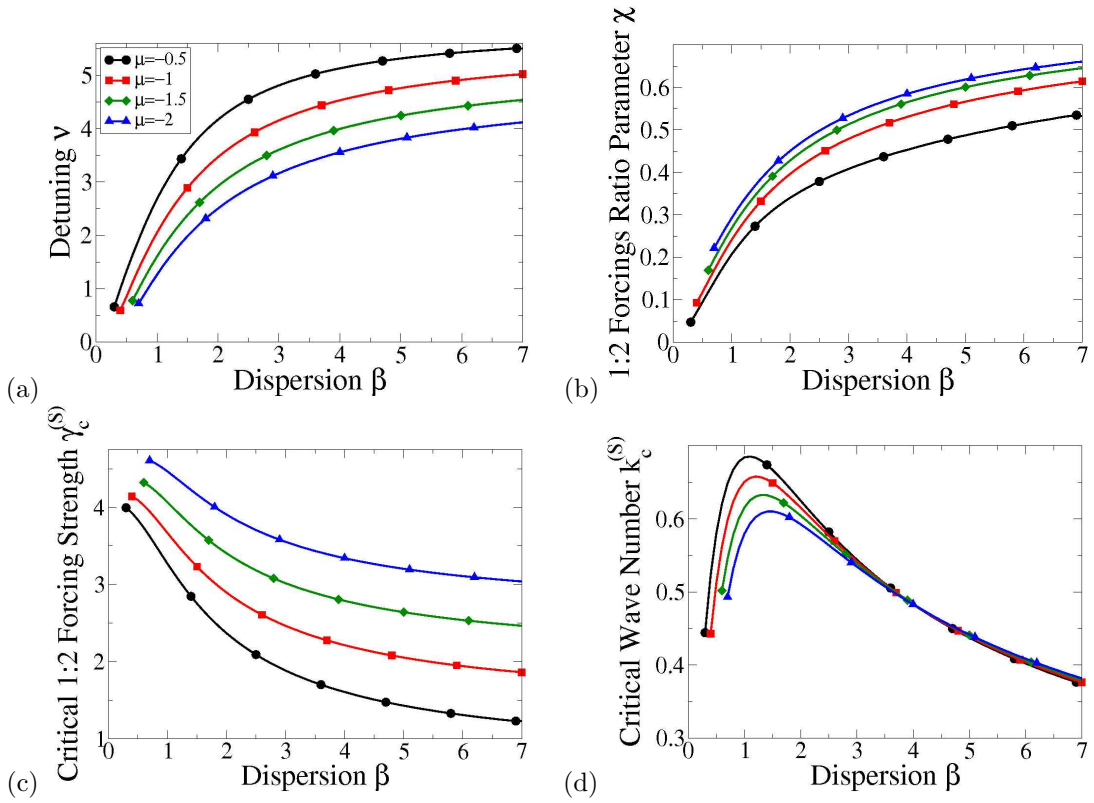

Figure 2: Linear parameters at the codimension-2 point $K = 2$ and $\gamma_c^{(H)} - \gamma_0^{(S)} \equiv 0.01$ for detuning $\sigma = 4$ as a function of the dispersion β and the damping μ. (a) Detuning ν, (b) forcing ratio χ, (c) critical forcing strength $\gamma_c^{(S)}$, and (d) critical wave number $k_c^{(S)}$

as

$$\begin{pmatrix} A_r \\ A_i \end{pmatrix} = \epsilon \left\{ \sum_{m=1}^{N} Z_m(T) \left(\sum_{n=-\infty}^{\infty} \begin{pmatrix} X_n \\ Y_n \end{pmatrix} e^{i(n+\frac{1}{2})\nu t} \right) e^{i\mathbf{k}_m \cdot \mathbf{x}} + c.c. \right\} + \epsilon^2 \begin{pmatrix} A_r^{(2)} \\ A_i^{(2)} \end{pmatrix} + \epsilon^3 \begin{pmatrix} A_r^{(3)} \\ A_i^{(3)} \end{pmatrix} + \ldots, \quad |\mathbf{k}_m| = k_c \tag{10}$$

where $0 < \epsilon \ll 1$ and the complex amplitudes $Z_m(T)$ depend on the slow time $T = \epsilon^2 t$. The corresponding wave vectors are denoted by $\mathbf{k}_m$. We also expand γ as $\gamma = \gamma_c + \epsilon^2 \gamma_2$.

A standard but lengthy calculation yields amplitude equations for the $Z_j(T)$ describing the $N-$mode pattern:

$$\frac{dZ_i}{dT} = \lambda \gamma_2 Z_i - \left(b_0 |Z_i|^2 + \sum_{j=1, j\neq i}^{N} b(\theta_{ij}) |Z_j|^2 \right) Z_i, \quad i = 1 \ldots N, \tag{11}$$

where θ_{ij} corresponds to the angle between the wave vectors $\mathbf{k}_i$ and $\mathbf{k}_j$. Note that there are no quadratic terms in (11), because these amplitude equations correspond to subharmonic patterns and must therefore be equivariant under the symmetry $Z_j \to -Z_j$. In order to have stable complex patterns made up of many modes, the competition between modes needs to be sufficiently weak. Since in the amplitude equations (11) only pairwise mode interactions arise, a minimal condition for complex patterns to be stable is the stability of rectangle patterns, which are comprised of 2 modes at some angle θ, with respect to stripes. This requires $|b(\theta)/b_0| < 1$.

The self- and cross-coupling coefficients, b_0 and $b(\theta_{ij})$, respectively, can be strongly influenced by resonant triad interactions as illustrated in Fig.3. There the black circles represent the subharmonic critical circle and the red circle the wavevector of the most weakly damped harmonic mode for a given choice of critical forcing γ. At quadratic order resonant triad interaction takes place through two mechanisms, each feeding into the coefficients at cubic order. The first mechanism is through the interaction of two different wave vectors ($\mathbf{k}_1 + \mathbf{k}_2$ in Fig.3a) seperated by an angle θ_r: the cross-coupling coefficient $b(\theta)$ is strongly impacted near $\theta = \theta_r$ if the mode excited at quadratic order through the interaction of these two wave vectors is weakly damped [19–22]. The angle θ_r is a function of the wavenumber ratio K, $\theta_r = 2\cos^{-1}(K/2)$. The second mechanism is through the interaction of a wave vector with itself ($2\mathbf{k}_1$ in Fig.3b): in this case, if the harmonic mode at $2\mathbf{k}_c$ is weakly damped, the self-coupling coefficient b_0 is strongly influenced [22, 23, 25]. In Fig.3a $K < 2$ ($\theta_r \neq 0$), so the mode excited by the vector $\mathbf{k}_1 + \mathbf{k}_2$ is weakly damped and the mode excited by the $2\mathbf{k}_1$ vector is strongly damped. In Fig.3b $K = 2$ ($\theta_r = 0$), so the opposite is true.

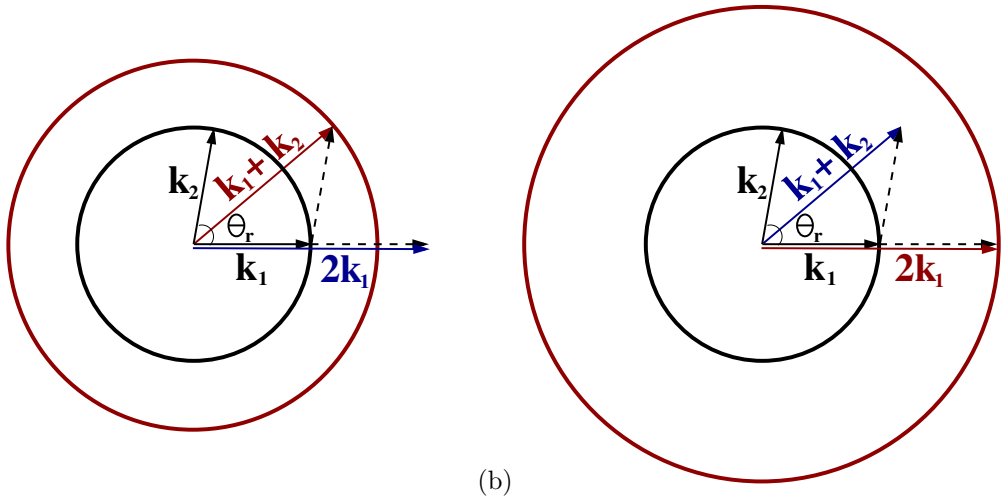

(a) (b)

Figure 3: Resonant triad interaction. Inner circle represents critical circle at $k_c^{(S)}$, outer circle represents weakly damped mode at (a) $K = 2\tan^{-2}(2/5)$, (b) $K = 2$. The wave vector $\mathbf{k}_1 + \mathbf{k}_2$ is relevant for $b(\theta)$ while $2\mathbf{k}_1$ affects b_0 (cf. eq.(11)).

Fig.4 shows the effect of the resonant triad interactions on the self-coupling coefficient b_0, by plotting b_0 as a function of the 1:3 forcing phase Φ for different values of the 1:3 forcing strength ρ. Fig.4a corresponds to the case illustrated in Fig.3a with $K = 2\cos(\tan^{-1}(2/5))$; with this choice of K the resonance angle $\theta_r \equiv 2\tan^{-1}(2/5)$ is near $\pi/4$ and the associated Fourier modes fall on a regular grid [47] for later comparison with numerical simulation. In Fig.4b $K = 2$ and the effect of the resonant triad on b_0 is greatly enhanced - note the difference in scale compared to Fig.4a - and even quite weak forcing ρ can change the sign of b_0 and with it the direction of the bifurcation to stripes. In the following we restrict ourselves to values of the phase Φ for which $b_0 > 0$ and the stripes bifurcate supercritically.

To assess the mode competition for $K = 2$, Fig.5 shows the dependence of the cross-coupling coefficient ratio $b(\theta)/b_0$ on θ. To enhance the stability of patterns comprised of multiple modes by maximizing the range of weak competition we maximize the damping b_0 and choose $\Phi = 3\pi/4$ (cf. Fig.4). Since $K = 2$, the self-coupling b_0 is enhanced by the resonant triad, while away from $\theta = \theta_r \equiv 0$ the cross-coupling $b(\theta)$ is only weakly affected. Thus, as expected, for $\rho \geq 1$ the ratio $b(\theta)/b_0$ is strongly reduced away from $\theta = 0$ allowing for rectangle patterns corresponding to angles as small as $\theta = \theta_c \sim 30°$ and smaller to be stable with respect to stripes. Consequently, patterns comprised of four or possibly even more modes are expected to be stable, as discussed in Sec.4.2.

The mode interaction also depends on the linear dispersion α and the nonlinear dispersion parameter β. These two parameters are system parameters that may not be tunable in experiments. It is therefore of interest to assess over what range in these parameters complex patterns are to be

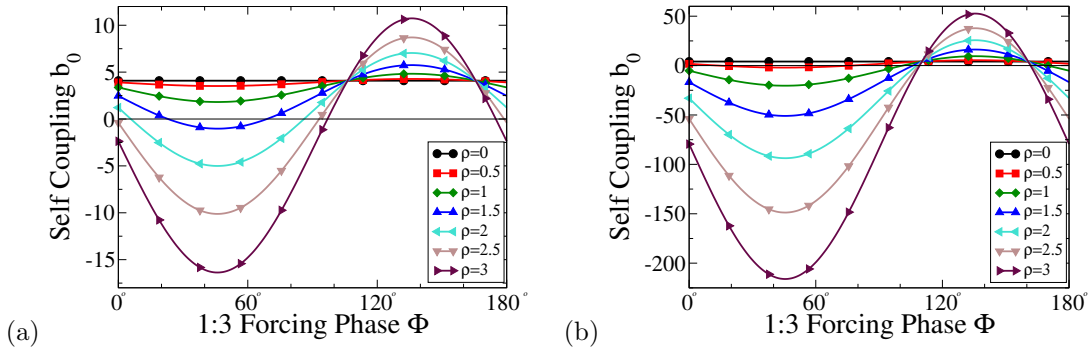

Figure 4: Self-coupling coefficient b_0 plotted against the 1:3 forcing phase Φ for various values of the 1:3-forcing strength ρ with $\alpha = -1$. (a) $K = 2\cos(\tan^{-1}(2/5)$, other parameters as in Fig.1a; (b) $K = 2$, other parameters as in Fig.1b.

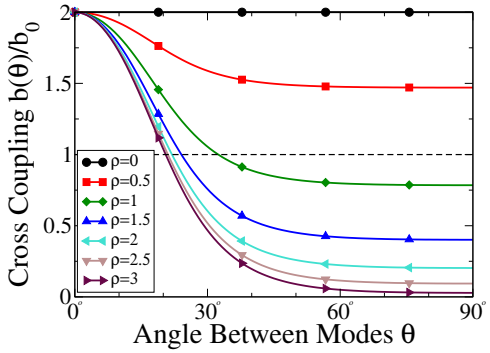

Figure 5: Coupling coefficient ratio $b(\theta)/b_0$ for $K = 2$ with $\Phi = 3\pi/4$ with linear parameters as in Fig.1b and nonlinear dispersion $\alpha = -1$ for different strengths of 1:3-forcing ρ. Rectangles are stable for $|b(\theta)/b_0| < 1$.

expected and to what extent the forcing parameters can be adjusted so as to reach the regions of interest for given system parameters.

The effect of the nonlinear dispersion parameter α on the ratio $b(\theta)/b_0$ is shown in Fig.6a for $\rho = 1$. Somewhat similar to the dependence on ρ, with increasing α the ratio $b(\theta)/b_0$ decreases and the range of θ for which rectangle patterns are stable increases. For more positive values of α even small forcing amplitudes ρ reduce the mode interaction significantly, but as ρ is increased the ratio $b(\theta)/b_0$ saturates at values that are not much smaller than shown in Fig.5 for $\alpha = -1$. In the simulations discussed in Sec.5 below we use a moderate value of $\alpha = -1$. For single-frequency forcing it was found that the self-coupling coefficient b_0 changes sign for $\alpha = \beta$, rendering the bifurcation subcritical for $\alpha > \beta$ [36]. Interestingly, with multi-frequency forcing the sign of b_0 depends also on the forcing strength ρ and, in fact, even for $\alpha = \beta$ the bifurcation to stripes can be made supercritical by increasing the forcing strength. This is illustrated in Fig.6b where b_0 is shown as a function of ρ for different values of α near $\beta = 3$.

To assess the dependence of the mode interaction on the linear dispersion coefficient β we do not perform a scan in β but rather focus on one other value, $\beta = 1.4$, which corresponds to the value found experimentally for the Belousov-Zhabotinsky reaction [48]. We adjust the forcing parameters χ and ν to stay at the codimension-2 point $K = 2$ and $\gamma_c^{(H)} - \gamma_0^{(S)} = 0.01$. The nonlinear dispersion coefficient was found in the experiments to be $\alpha = -0.4$. Since the functional form of the angle dependence of $b(\theta)$ does not change much with the parameters we use the minimal angle θ_c for which rectangles are still stable with respect to stripes as a proxy for the strength of the mode competition. Thus $b(\theta_c)/b_0 = 1$. In Fig.7 we show θ_c as a function of the forcing strength ρ for various values of the overall detuning σ. Clearly, even for these experimentally relevant parameters the resonant triad

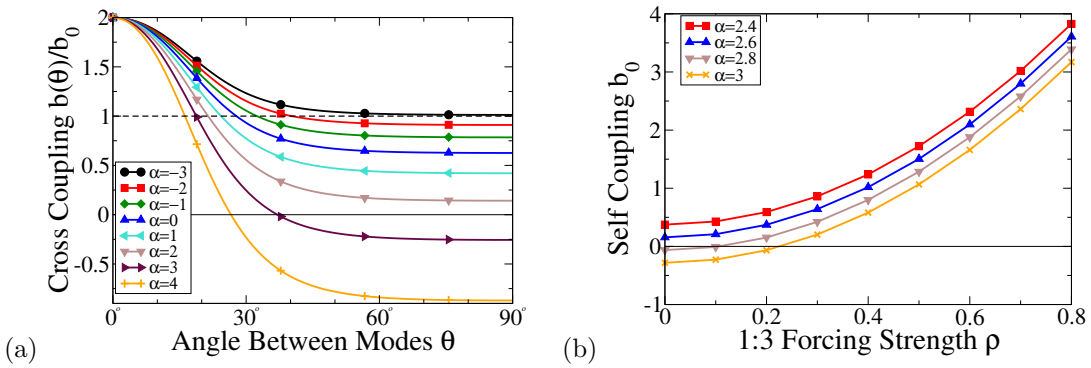

Figure 6: Coupling coefficient ratio $b(\theta)/b_0$ (a) and self-coupling b_0 (b) for $K = 2$ and $\Phi = 3\pi/4$ with parameters as in Fig.1b for 1:3 forcing strength $\rho = 1$ and different values of the nonlinear dispersion parameter α.

interaction can be exploited to make the mode competition sufficiently weak to stabilize rectangle patterns over a wide range of angles. This suggests that multi-mode patterns should become stable for moderate values of the forcing parameters, which is confirmed below.

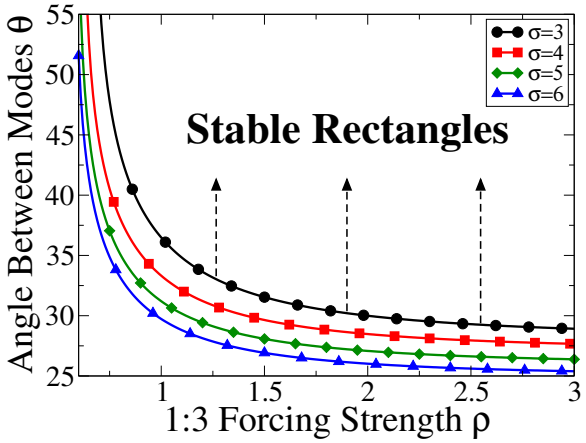

Figure 7: Belousov-Zhabotinsky case. Minimal angle θ_c for which rectangles are stable to stripes ($b(\theta_c)/b_0 = 1$) as a function of the 1:3-forcing strength ρ for different values of the detuning σ. Parameters $\mu = -1$, $\alpha = -0.4$, $\beta = 1.4$ with χ and ν tuned to the codimension-2 point $K = 2$ and $\gamma_c^{(H)} - \gamma_0^{(S)} = 0.01$. .

For $K = 2\cos(\tan^{-1}(2/5))$ the resonant triad affects mostly $b(\theta)$ rather than b_0. Fig.8 shows the resulting ratio $b(\theta)/b_0$ as a function of the angle θ. To ensure $b_0 > 0$ we use again $\Phi = 3\pi/4$. As expected $b(\theta)/b_0$ exhibits a prominent peak near $\theta = \theta_r = 2\tan^{-1}(2/5)$. As in Fig.5 the enhancement is increased with ρ (Fig.8a), and as α becomes more positive (Fig.8b). We also see from these plots that the range for which $b(\theta)/b_0 < 1$, that is, the range of stable rectangles, is limited to $60^\circ \lesssim \theta < 90^\circ$. Thus, we anticipate only stripe, square or hexagon patterns to be stable in this regime.

For $K = 2\cos(\tan^{-1}(2/5))$ the competition between modes subtending an angle near θ_r is strongly enhanced for values of the 1:3-forcing phase near $\Phi = 3\pi/4$ resulting in a suppression of θ_r-rectangles. For the same K but $\Phi = \pi/4$, we expect correspondingly a selective enhancement of the θ_r-rectangles as long as ρ is sufficiently small so that $b_0 > 0$ (see Fig.4). This is shown in Fig.9, which depicts the behaviour of the cubic coupling coefficient ratio as a function of the angle θ for different values of the 1:3-forcing strength ρ and of the nonlinear dispersion α in this regime. As the 1:3-forcing strength ρ is increased, and as the nonlinear dispersion α becomes more positive,

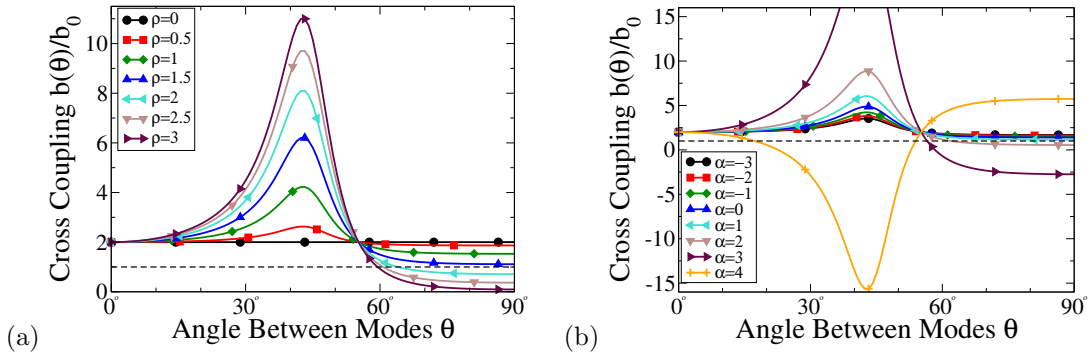

(a) (b)

Figure 8: Coupling coefficient ratios for $K = 2\cos(\tan^{-1}(2/5))$ and $\Phi = 3\pi/4$ with parameters as in Fig.1a for (a) nonlinear dispersion parameter $\alpha = -1$ and different strengths of 1:3-forcing ρ and (b) 1:3 forcing strength $\rho = 1$ and different values of the nonlinear dispersion parameter α.

the dip with minimum at $\theta = \theta_r = 2\tan^{-1}(2/5)$ becomes more and more pronounced. In parallel the range in θ of stable rectangle patterns increases around θ_r. Due to the narrowness of the dip we expect at most stripe and θ_r-rectangle patterns to be stable. For values of ρ and α such that $b(\theta)/b_0 < -1$ the corresponding rectangles pattern become subcritical and our weakly nonlinear analysis to cubic order is insufficient to make predictions about pattern selection involving those modes.

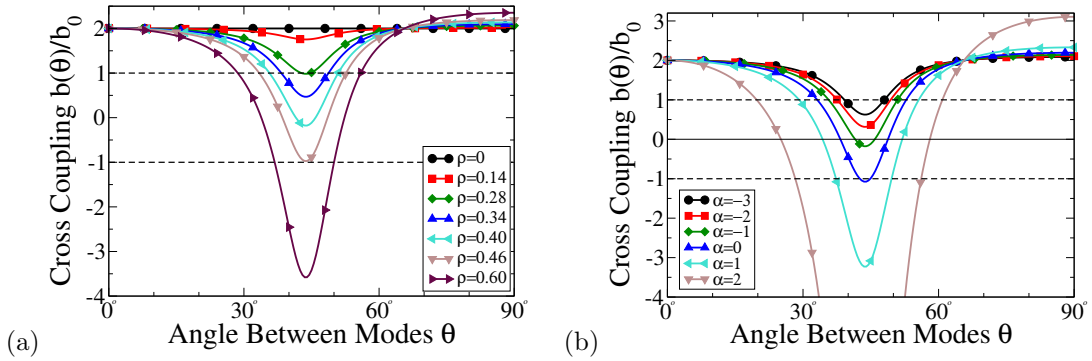

(a) (b)

Figure 9: Coupling coefficient ratios for $K = 2\cos(\tan^{-1}(2/5))$ and $\Phi = \pi/4$ with parameters as in Fig.1a for (a) nonlinear dispersion parameter $\alpha = -1$ and different strengths of 1:3-forcing ρ and (b) 1:3 forcing strength $\rho = 1$ and different values of the nonlinear dispersion parameter α.

4.2 Competition between complex patterns

If multiple patterns are simultaneously linearly stable they can coexist and compete in sufficently large systems. Typically they form then domains and the competition involves the motion of walls separating the domains. If the system allows a Lyapunov functional this competition can be characterized in terms of the difference between the energies associated with the respective patterns. Unless the domain walls become pinned by the underlying pattern [49, 50], it is expected that the final state arising from random initial conditions consists of the pattern with minimal energy [28,51].

Because $b(\theta_{ij}) = b(\theta_{ji})$, (11) can indeed be derived from a Lyapunov functional $\mathcal{F}$, such that $\frac{\partial Z_j}{\partial T} = -\frac{\partial \mathcal{F}}{\partial \bar{Z}_j}$ with

$$\mathcal{F} = \sum_{n=1}^{N} \left[-\lambda(\gamma - \gamma_c)|Z_n|^2 - \frac{1}{2}(b_0|Z_n|^4 + \sum_{m=1, m\neq n}^{N} b(\theta_{mn})|Z_n|^2|Z_m|^2 \right] \tag{12}$$

for a pattern with N modes. The Lyapunov function gives the energy $\mathcal{F}_{\mathcal{N}}$ for an equal-amplitude $N-$mode pattern, which we rescale to obtain $\hat{\mathcal{F}}_N$,

$$\hat{\mathcal{F}}_N \equiv \frac{\mathcal{F}_N}{(\gamma-\gamma_c)^2} = \frac{-\lambda^2}{b_0 + \sum_{n=1,n\neq j}^{N} b(\theta_{jn})}, \tag{13}$$

for some $j \in [1, N]$. The sum in the denominator represents the sum of all cubic coefficients in (11). Since the modes are evenly spaced, the choice of j in (13) is arbitrary. We use the energy $\mathcal{F}_{\mathcal{N}}$ as a guide to predict which N-mode pattern will ultimately emerge.

Figs.10-13 show how the energies $\hat{\mathcal{F}}_{\mathcal{N}}$ vary with ρ, the strength of forcing near 1:3 resonance, for different patterns with N modes evenly spaced in Fourier space. Since the energy depends smoothly on the angles θ_{jn} (cf. (13)) little change in the energy is expected if the modes are not quite evenly spaced.

For $K = 2$ and $\alpha = -1$ the energies of the patterns with more than 3 modes are very close to each other, as seen in Fig.10a. For clarity we show therefore in Fig.10b the difference $\hat{\mathcal{F}}_N - \hat{\mathcal{F}}_4$. As one increases ρ, first stripe patterns ($N = 1$), then square patterns ($N = 2$), then hexagons ($N = 3$), and eventually supersquares ($N = 4$) have the lowest energy. For the respective parameter values, these are therefore the patterns we expect eventually to arise from noisy initial conditions. Also indicated in Figs.10a,b is the linear stability of these patterns. Here we determine the linear stability of an N-mode pattern by calculating the linear stability of that pattern within the space spanned by the N evenly spaced modes and an additional mode rotated an arbitrary angle ψ with respect to the $\mathbf{k}_1$-mode in Fourier space. For larger ρ patterns comprised of 5 and 6 modes are linearly stable but do not have the lowest energy, though for $\rho > 2$ the energies of the patterns with 4 and 5 modes are very close.

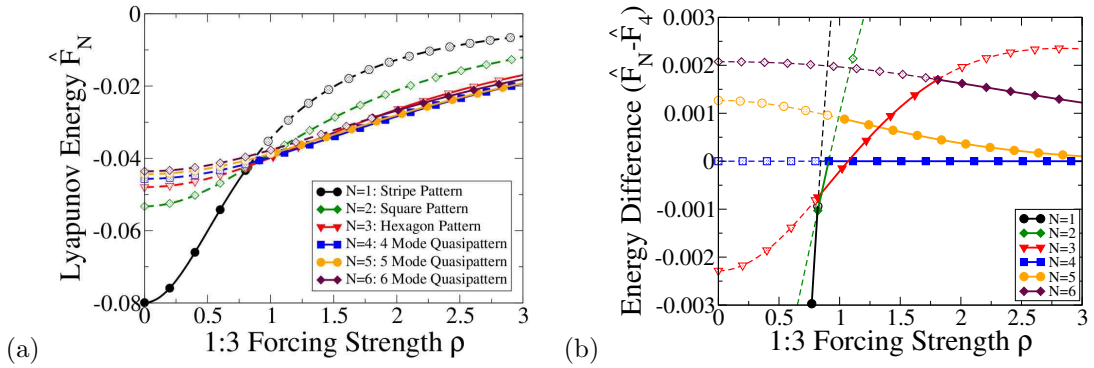

Figure 10: (a) Rescaled energies $\hat{\mathcal{F}}_N$ for evenly spaced modes in the case $K = 2$. Parameters as in Fig.1b with $\alpha = -1$ and $\Phi = 3\pi/4$. Solid (dashed) lines denote linearly stable (unstable) patterns. (b) Energy difference $\hat{\mathcal{F}}_N - \hat{\mathcal{F}}_4$ for the same data as shown in (a). The 4-mode pattern is preferred for $\rho > 1.2$.

In Sec.4.1 we showed that for a more positive α relatively small values of the 1:3-forcing strength ρ are sufficient to stabilize rectangle patterns over a wide range of θ (cf. Fig. 6a). As a result we expect that the resonant triad can stabilize patterns comprised of more modes than was possible in the case $\alpha = -1$ depicted above. Fig.11b shows that this is indeed the case. Increasing α to $\alpha = 2.5$ reduces for $\rho > 1$ the energy of the 5-mode patterns below that of the 4-mode pattern and renders it the pattern with the lowest energy among the patterns with equally spaced modes. We therefore expect that in numerical simulations 5-mode patterns would arise over a large range in ρ.

For the parameter set that is relevant for the Belousov-Zhabotinsky reaction [48] we found that the mode competition is also sufficiently reduced to suggest the stability of multi-mode patterns (cf. Fig.7). This is confirmed in Fig.12, which shows the energies for $\alpha = -0.4$ and $\beta = 1.4$. While for $\sigma = 4$ the 4-mode pattern has an energy that is only barely below that of the hexagons and reaches those lower values only for large forcing strengths ρ (Fig.12), increasing σ to $\sigma = 6$ pushes

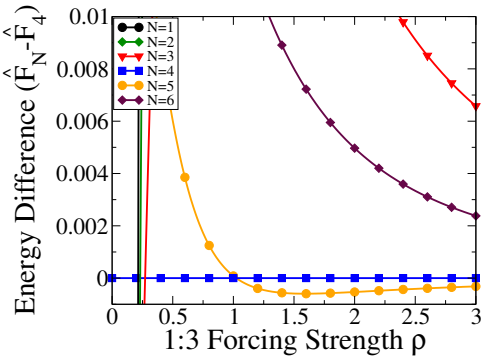

Figure 11: Rescaled energies $\hat{\mathcal{F}_N}$ for evenly spaced modes in the case $K = 2$. Parameters as in Fig.1b with $\alpha = 2.5$ and $\Phi = 3\pi/4$. 5-mode pattern preferred for $\rho > 1$.

the energy of the 4-mode pattern well below that of the hexagons (Fig.12b). We therefore expect that the complex patterns we discuss in this paper are accessible in this experimental system.

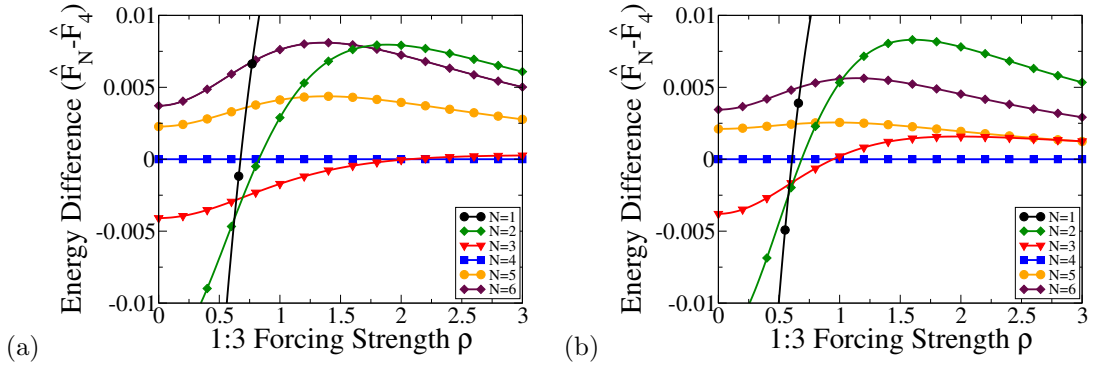

Figure 12: Pattern selection for Belousov-Zhabotinsky parameters [48]. Rescaled energy difference $\hat{\mathcal{F}_N} - \hat{\mathcal{F}_4}$ for N evenly spaced modes. Here $\alpha = -0.4$, $\beta = 1.4$, $\sigma = 4$ (a) and $\sigma = 6$ (b).

For $K = 2\cos(\tan^{-1}(2/5))$ with $\Phi = 3\pi/4$ (Fig.13a), stripes are again stable for small ρ. As ρ is increased stripes lose stability and square patterns ($N = 2$) become linearly stable and have the lowest energy beyond $\rho \approx 1.6$. Hexagon patterns ($N = 3$) become linearly stable at $\rho = 2.7$, but do not have lower energy than the square patterns. Patterns with more than 3 modes are linearly unstable, which is consistent with the predictions based on the coupling coefficient shown in Fig.8a: Fourier modes subtending angles smaller than $\pi/3$ compete strongly and therefore do not coexist stably. In simulations starting from random initial conditions, we therefore expect either stripe patterns (for $\rho < 1.6$) or square patterns to arise. For $\Phi = \pi/4$, shown in Fig.13b, stripes again are stable and have the lowest energy for small ρ. For $\rho = 0.28$ they become unstable to rectangle patterns spanned by modes subtending an angle of $\theta = \theta_r \equiv 2\tan^{-1}(2/5)$. As ρ is increased to $\rho = 0.46$ this rectangle pattern becomes subcritical (cf. Fig.9) and the weakly nonlinear analysis taken to cubic order and the associated energy arguments are not sufficient to make predictions about pattern selection. For $\rho > 0.28$ none of the patterns with equally spaced modes has lower energy than the rectangle pattern selected by the resonant triad. Note that in the cubic truncation (13) the energy for a pattern diverges when the respective bifurcation changes direction.

5 Numerical Simulations in Large Domains

To confirm our predictions for the pattern selection, we perform numerical simulations of the complex Ginzburg-Landau equation (6). Being interested in the formation of complex patterns comprised of

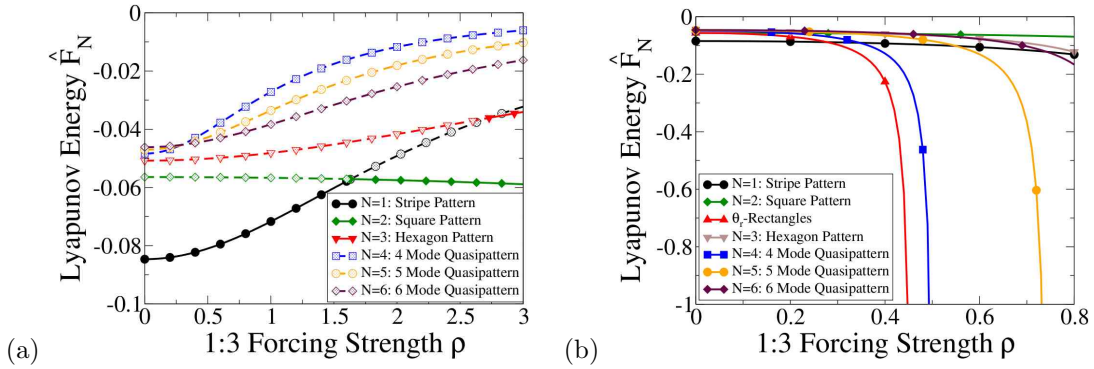

Figure 13: Rescaled energies $\hat{\mathcal{F}_N}$ for evenly spaced modes in the case $K = 2\cos(\tan^{-1}(2/5))$. Parameters as in Fig.1a with $\alpha = -1$ and (a) $\Phi = 3\pi/4$ (cf. Fig.8), (b) $\Phi = \pi/4$ (cf. Fig.9). In (a), solid (dashed) lines denote linearly stable (unstable) patterns.

3 or more modes, we focus on the case $K = 2$. The linear parameters are as in Fig.1a with nonlinear parameters $\alpha = -1$, $\Phi = 3\pi/4$, and various values of ρ. We use periodic boundary conditions and employ a pseudo-spectral method with Crank-Nicolson-Adams-Bashforth time stepping

First, to test the weakly nonlinear analysis we focus on the regime where both hexagons and 4-mode patterns are linearly stable (Fig.10) and run numerical simulations in domains of minimal size for each pattern. Thus, all participating modes lie exactly on the critical circle. Since the 4-mode pattern with evenly spaced modes does not lie on a regular Fourier grid we approximate it by modes spaced at $\theta_1 = 2\tan^{-1}(1/2) \approx 53^\circ$ and $\theta_2 = \pi/2 - 2\tan^{-1}(1/2) \approx 37^\circ$ apart. Due to the smooth dependence of the energy on the angles θ_{jn} (cf. Eq.(13)) little change in the energy is expected if the modes are not quite evenly spaced. From Fig.10b, for a 1:3-forcing strength $\rho = 1$ hexagons and 4-mode patterns are both linearly stable to stripes and the 4-mode patterns are also linearly stable to square patterns. The numerical simulations confirm these stability predictions. Starting with a noisy initial condition generated from a uniform distribution with amplitude 0.05 we get as expected hexagons (Fig.14a) and supersquares (Fig.14b). Fig.14 also illustrates the slight diffference in the domain sizes used in the simulations, which are required to accomodate the patterns.

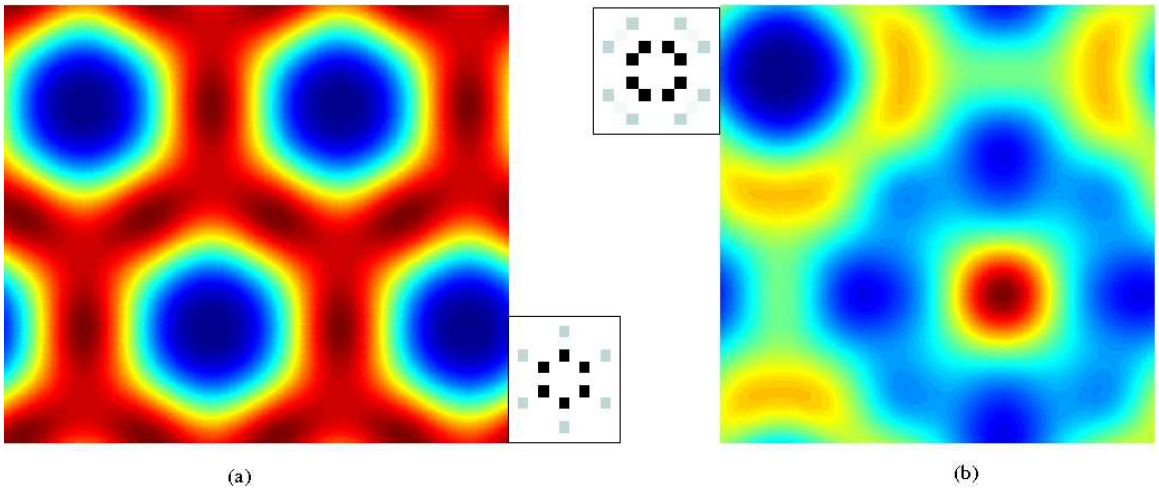

Figure 14: Small-system numerical simulations of (6) for 1:3 forcing strength $\rho = 1$. (a) Hexagon pattern in rectangular domain, $L_x = 4\pi/k^{SH} \approx 23.49$, $L_y = L_x/\sqrt{3} \approx 13.56$. (b) Supersquare pattern in square domain, $L = 2\pi/(\cos(\tan^{-1}(1/2))k^{(SH)} \approx 13.13$. Parameters as in Fig.1b (case $K = 2$) with $\alpha = -1$, $\Phi = 3\pi/4$.

To investigate the competition between N-mode patterns with different values of N in the same computational domain we perform simulations in a large system of linear size $L_x = L_y \equiv L$, given below, representing 40 wavelengths. Fig.10b shows that near $\rho = 1$ hexagons and 4-mode patterns are both linearly stable, but the pattern with minimal energy depends on ρ. In order to investigate the competition between these planforms we start each simulation with the same noisy initial condition, generated from a uniform distribution with amplitude 0.01, and vary only ρ. Moreover, in order to clearly identify the *nonlinear* competition between hexagons and 4-mode patterns and its dependence on ρ, we choose L such that the Fourier modes with $\theta = \pi/3$ and $\theta = \pi/4$ have the same growth rates. This is achieved by taking $L = 40(2\pi/(k^{(SH)} - d)) \approx 473.39$ for which the modes for the hexagons and the 4-mode patterns are at an equal distance $d = 0.004159$ on opposite sides of the critical circle.

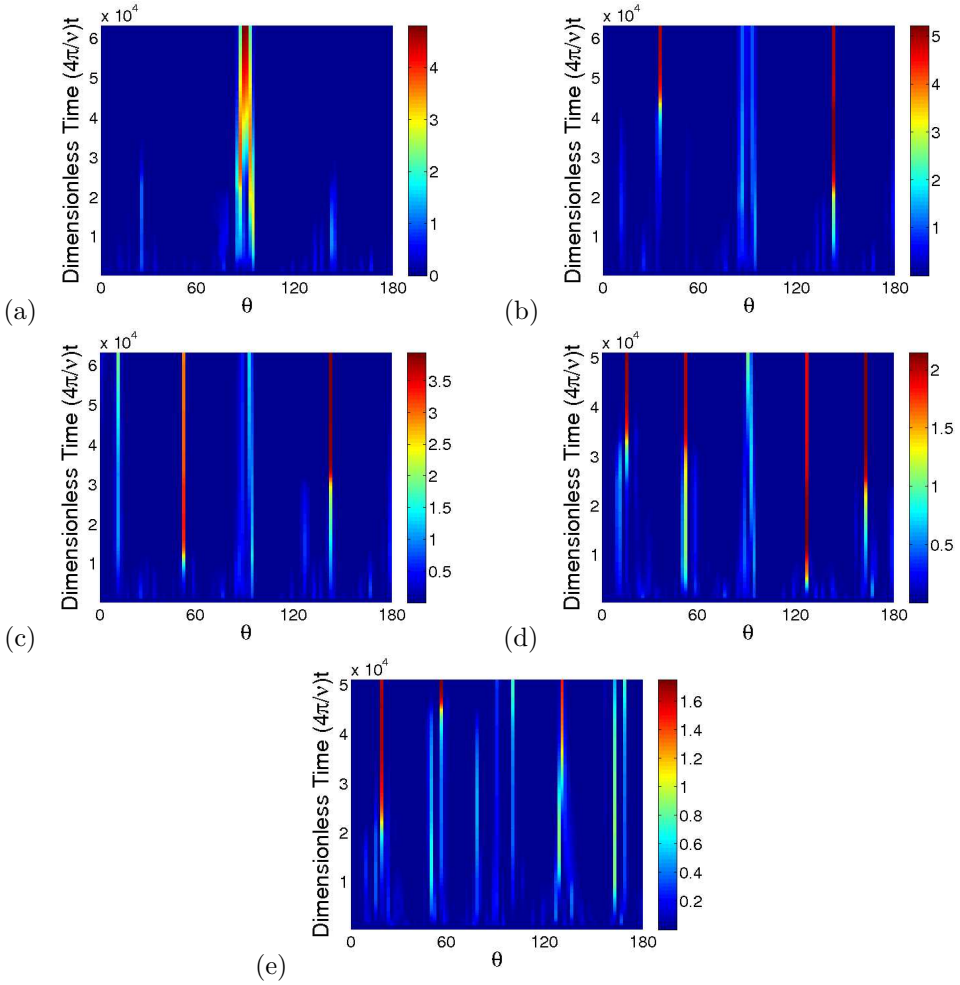

Figure 15: Strobed time dependence of the power spectrum in an annulus around the critical circle for varying 1:3 forcing strengths ρ. Parameters as in Fig.1b with $\alpha = -1$ and $\Phi = 3\pi/4$. All simulations use the same noisy initial condition. (a) $\rho = 0.8$, (b) $\rho = 1$, (c) $\rho = 1.2$, (d) $\rho = 2$, (e) $\rho = 3$.

To visualize the competition between the modes near the critical circle, Fig.15 shows the temporal evolution of the magnitude of the Fourier modes inside a narrow annulus around the critical circle, divided into bins with an angular width of 2° plotted stroboscopically at multiples of the period $4\pi/\nu$. For $\rho = 0.8$, based on energy arguments and the linear stability illustrated in Fig.10b, we anticipate the final state to consist of a stripe pattern. This is confirmed by the numerical simulation. While in the Fourier transform Fig.15a initially three modes come up, reflecting the linear stability of

hexagons for $\rho = 0.8$, ultimately the pattern with lower energy, stripes, dominates and only a single mode remains. The competition can also be seen in in TimeEvolutionMovie_rhoIs0p8.mov, which shows the temporal evolution of the full pattern strobed with period $4\pi/\nu$. More careful inspection shows that the middle peak, which seems weaker, actually consists of two modes of lesser strength that are slowly converging to a single strong peak. The splitting of the peak into two modes reflects a slight undulation of the resulting pattern, which is apparent in the snapshot of part of the final solution shown in Fig.16a.

Fig.15b shows the evolution of the Fourier transform for $\rho = 1$ corresponding to the time evolution of the full pattern shown in TimeEvolutionMovie_rhoIs1.mov. As with the $\rho = 0.8$ case, initially the amplitudes of three modes grow. In contrast to the $\rho = 0.8$ case, however, for $\rho = 1$ stripes are unstable to hexagons, and hexagons have the lowest energy. Correspondingly the three modes persist resulting in the hexagon patterns shown in Fig.16b. Note that the hexagon patterns are comprised of domains of up- and down-hexagons characterized by white and black centers, respectively. This reflects the fact that the amplitude equations (11) for these subharmonic patterns have no quadratic term, so neither the up- nor the down-hexagons are preferred. Whether eventually one of the two types wins out over the other depends on the interaction between the fronts connecting the domains.

For $\rho = 1.2$ we anticipate from Fig.10b that the resulting solution will be a 4-mode pattern. Indeed, Fig.15c shows 4 modes in the Fourier transform, though they are not quite equally spaced. The corresponding pattern evolution is shown in TimeEvolutionMovie_rhoIs1p2.mov; Fig.16c shows the final state, characterized by supersquare (dash-dotted, blue circle) and antisquare (dashed, yellow circles) elements with approximate 4-fold rotational symmetry [52], as well as approximate 8-fold symmetric elements (solid, white circle).

From Fig.10b a 4-mode pattern is also anticipated for $\rho = 2$, but the numerical simulation actually results in a 5-mode pattern as shown in Fig.15d. The energies for evenly-spaced 4- and 5-mode patterns are very close for this forcing strength. Therefore changes in the energies that result from an uneven distribution of the modes may render the 5-mode pattern energetically lower. The corresponding pattern features elements with approximately 5- and 10-fold rotational symmetry (dashed,yellow and solid, white circles, respectively, in Fig.16d). For $\rho = 3$ even more modes persist for a long time and at the final time shown, $4\pi t/\nu = 5 \cdot 10^4$, the pattern has not settled yet into its final state. The temporal evolution of the full patterns for $\rho = 2$ and $\rho = 3$ are shown in TimeEvolutionMovie_rhoIs2.mov and TimeEvolutionMovie_rhoIs3.mov, respectively.

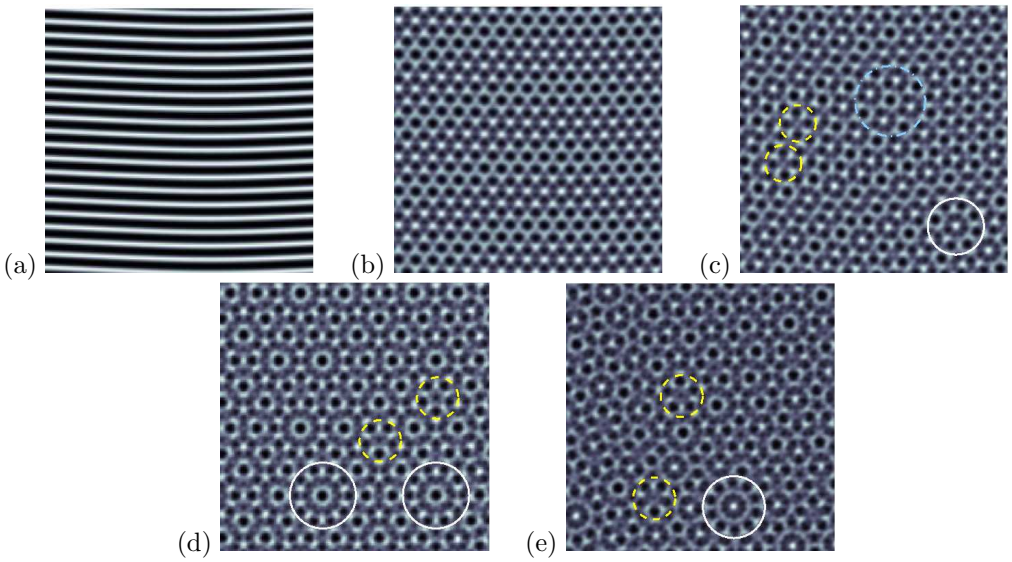

Figure 16: Zoom view ($0.25L \times 0.25L$) of final state at time $4\pi t/\nu = 5 \cdot 10^4$ for varying values of 1:3 forcing ρ with $L = 40(2\pi/(k^{(SH)} - d)) \approx 473.39$. Other parameters as in Fig.1b (case $K = 2$) with $\alpha = -1$, $\Phi = 3\pi/4$. The circles mark characteristic features of the patterns. (a) $\rho = 0.8$, (b) $\rho = 1$, (c) $\rho = 1.2$, (d) $\rho = 2$, (e) $\rho = 3$.

To characterize the ordering process taking place in the evolution of the patterns we calculate the spectral pattern entropy $S = \sum_{i,j} p_{ij} \ln p_{ij}$, where $p_{ij} = \tilde{p_{ij}}/(\sum_{i,j} \tilde{p}_{ij})$ is the normalized power in the Fourier mode with amplitude $\tilde{p}_{ij}$ and the sum includes all modes within the critical annulus binned into 10° segments. The entropy allows an estimate of the effective number of Fourier modes e^Scontributing to the pattern. Fig.17 illustrates the temporal evolution of e^S for different values of the 1:3 forcing strength ρ. The number of significant modes increases with ρ, although not monotonically for all times: for example, the curves corresponding to $\rho = 1$ and $\rho = 1.2$ cross several times, near dimensionless times $\nu t/4\pi = 12 \times 10^3, 17 \times 10^3, 35 \times 10^3$, before beginning to converge smoothly to $e^S \approx 3$ and 4, respectively. While the decrease in the effective number of Fourier modes with time in the transients is monotonic it occurs in spurts. For $\rho = 3$, for instance, there is a sudden dip near dimensionless time $\nu t/4\pi = 45 \times 10^3$. These dips are related to the sudden disappearance of modes that is apparent in the time evolution plots Fig.15a-e.

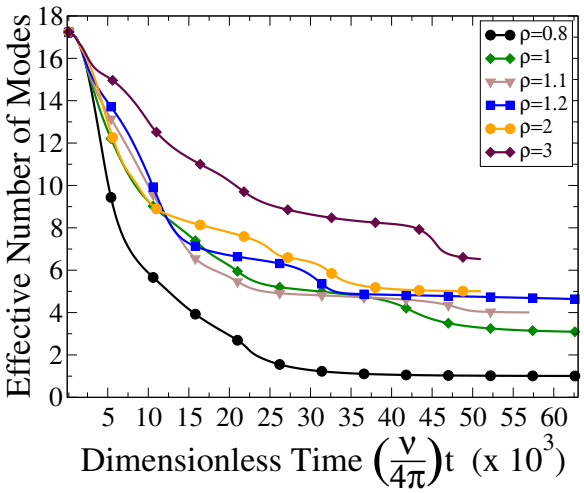

Figure 17: Effective number of Fourier modes e^S plotted as a function of time for different values of the 1:3 forcing strength ρ. Data taken from numerical simulations of (6) for parameters as in Fig.1b (case $K = 2$) with $\alpha = -1$, $\Phi = 3\pi/4$.

The complex Ginzburg-Landau equation (6) describes the evolution of the oscillation amplitude on a slow time. The full time evolution of the underlying system involves also the Hopf frequency. To illustrate the full time dependence the movie SimulationOver2Periods_withFastOscs.mov shows the evolution of the pattern over two forcing periods obtained for $\rho = 2$ as one might see it in an experiment. Fig.18 shows the corresponding temporal evolution of the real and imaginary parts of one of the spatial Fourier modes. The beating reflects the quasi-periodic forcing of the system. Details about the quantity shown in the movie SimulationOver2Periods_withFastOscs.mov and in Fig.18 are given in the Appendix.

6 Conclusion

We have demonstrated analytically and confirmed numerically that in systems that are near a Hopf bifurcation to spatially uniform oscillations forcing with judiciously chosen waveforms can stabilize complex periodic and quasi-periodic patterns comprised of up to 4 and 5 Fourier modes. Essential for the success of this approach was the use of a quasi-periodic forcing function in which the frequency content near twice the Hopf frequency consists of two frequencies; thus, the forcing is slowly modulated in time. Since the investigated complex patterns are subharmonic in time with respect to that modulation they arise in a pitch-fork bifurcation and are amenable to a weakly nonlinear analysis. The stabilization of the complex patterns was achieved by exploiting resonant triad interactions that result from the additional forcing component with a frequency close to three

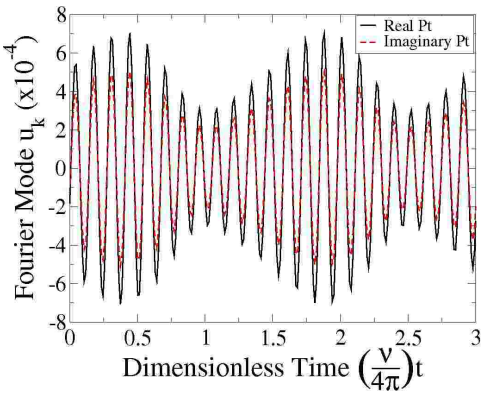

Figure 18: Temporal evolution of the real and imaginary parts of one of the spatial Fourier modes of the pattern shown in Fig.16e and in the movie SimulationOver2Periods_withFastOscs.mov.

times the Hopf frequency.

As expected from investigations in the context of the Faraday system [19, 24–26, 28, 53], our weakly nonlinear analysis showed that the resonant triad interaction can significantly modify the competition between Fourier modes of different orientation through the excitation of weakly damped modes. This damping is controlled by the differences in frequency and by the amplitude of the two forcing components near twice the Hopf frequency. It can be chosen to enhance the self-coupling of the modes significantly, which effectively reduces the competition between modes over a quite wide range of angles subtended by those modes. As in the Faraday system, this stabilizes complex patterns in the forced oscillatory systems investigated here. Alternatively, the forcing can be chosen to reduce the competition between modes differing in their orientation be a quite specific angle θ_r, which can be tuned over quite some range. In the Faraday system this approach can also lead to complex 4-mode patterns, which effectively consist of the combination of two square patterns that are rotated by an angle close to θ_r. In the forced oscillatory systems investigated here this mechanism alone does not yield complex patterns since in the unforced system squares are never stable, while in the Faraday system square patterns are stable for low viscosity [4, 23, 24]. Thus, in the present context this mechanism only leads to the stabilization of rectangle patterns. For sufficiently strong forcing their bifurcation can even be made subcritical, even though the stripe patterns (and the Hopf bifurcation itself) are supercritical.

We have complemented the weakly nonlinear analysis by direct simulations of the extended complex Ginzburg-Landau equation in large domains to study the competition between different, linearly stable, complex patterns. As expected from the variational character of the amplitude equations and the dependence of the energy of the various patterns on the forcing strength, we find that as the resonant triad interaction is increased more complex patterns dominate over simpler patterns. For the parameters chosen in the numerical simulations we find patterns with 4-fold symmetric elements reminiscent of super-squares and anti-squares [52] as well as 5-fold symmetric elements. The weakly nonlinear analysis (see Fig.5b) suggests that for other system parameters patterns comprised of more modes yet could be stable.

It should be noted that we reached the regime in which complex patterns are stable by tuning the amplitudes and phases of the forcing function, which constitute external forcing parameters. Therefore we expect that the complex patterns should be accessible quite generally in forced oscillatory systems, in particular also in chemical oscillators [37, 40, 54]. Specifically, our weakly nonlinear analysis indicates that the dependence of the patterns on the nonlinear dispersion coefficient α of the unforced system can be compensated by the strength of the forcing close to three times the Hopf frequency (cf. Fig.5b). Moreover, for the parameters determined experimentally in the oscillatory Belousov-Zhabotinsky reaction [48] we have shown explicitly that moderate forcing strengths are sufficient to stabilize 4-mode patterns. It should be noted, however, that the complex patterns possibly arise only very close to onset. Therefore the application of our results to experiments may require

systems with relatively large aspect ratios and a very careful tuning of the forcing parameters.

To characterize the temporal evolution of the patterns starting from random initial conditions and to distinguish the resulting patterns quantitatively we used the spectral entropy of the patterns, which quantifies the effective number of Fourier modes of the patterns. It allowed a clear distinction between patterns with three, four, or more significant modes. However a more detailed quantitative characterization of the transients that captures also the competition between multi-mode structures like super-squares and anti-squares, which have the same number of participating modes, is still an open problem (cf. [55]). The long-time scaling of the ordering process of such complex structures and a comparison with the ordering in stripe [56,57] or hexagon patterns [58] may also be interesting to study. Most likely, the number of different types of defects and their mutual interaction may play an important role. However, for the subharmonic patterns discussed here the amplitude equations do not contain any terms of even order. Therefore the strong interaction between defects that is associated with those terms and that should make their dynamics in particular interesting in the case of 5-mode patterns [59] will not be present here.

Here our focus was on systems below the Hopf bifurcation ($\mu < 0$). It would be interesting to pursue a similar study above the Hopf bifurcation. There the spontaneous oscillations, which do not arise in the Faraday system, and their competition with phase-locked patterns driven by the forcing may lead to additional complexity. For single-frequency forcing above the Hopf bifurcation, labyrinthine stripe patterns arise from the oscillations through front instabilities and stripe nucleation [54]. It is unknown what happens if the stripes are unstable to the more complex patterns discussed here.

It would also be interesting to consider opposite signs for the detunings ν_{21} and ν_{22} of the 1 : 2-forcing, frequency so that one of the detunings is just above the Hopf frequency, and the other just below. Then only one of the two forcing terms will yield a pattern-forming instability [36], while the other term will induce a phase-locking of spatially homogeneous oscillations. The result of the interaction between these two instabilities is not known.

Finally, we did not explore the subcritical cases $b_0 < 0$ or $b(\theta)/b_0 < -1$. The weakly nonlinear analysis to cubic order is insufficient to make predictions about pattern selection in these cases. Fig.9 suggests that for $K = 2\cos(\tan^{-1}(2/5))$ large-amplitude rectangle patterns with θ close to $\theta_r = \tan^{-1}(2/5)$ could be stabilized by the forcing

We gratefully acknowledge discussions with A. Rucklidge and M. Silber. This work was supported by NSF grants DMS-322807 and DMS-0309657.

Appendix

In Section 2 we derived the form of the extended CGLE (6) based on symmetry arguments. To illustrate that the additional terms arise from a general forcing function in a natural way we derive the coefficients of the equation here for the Brusselator, which often has served as a simple model for chemical oscillations [39]. With the forcing included it can be written as

$$\begin{aligned}\frac{\partial u}{\partial \tilde{t}} &= 1-(1+B)u+D_u\Delta u+\big(1+f_2(\cos(\chi)\sin((2+\nu_{21})\tilde{t})+\sin(\chi)\sin((2+\nu_{22})\tilde{t}))+ \quad (14)\\ &\quad +f_1\sin((1+\nu_1)\tilde{t})+f_3\sin((3+\nu_3)t)\big)\,u^2v,\\ \frac{\partial v}{\partial \tilde{t}} &= Bu+D_v\Delta v-u^2v, \quad (15)\end{aligned}$$

where u and v represent two reacting and diffusing chemical species. In the formulation (14,15), which differs slightly from the form presented in [39] in the coefficients of the linear terms, the Hopf bifurcation occurs at $B = 2$ and the Hopf frequency is given by $\omega = 1$. The small parameters $\nu_j = O(\delta^2)$, $\delta \ll 1$, represent the detuning (cf. eqs.(3,4)), the parameters $f_1 \equiv \delta^3\hat{f}_1$, $f_2 \equiv \delta\hat{f}_2$, and $f_3 \equiv \delta\hat{f}_3$ represent the small 1:1-, 1:2-, and 1:3 forcing strengths with $\hat{f}_j = \mathcal{O}(1)$, and the parameters D_u and D_v are the diffusion coefficients. To derive the extended CGLE (6) we expand (14,15) near

the Hopf bifurcation about the basic state $(u, v) = (1, B)$ as

$$\begin{pmatrix} u \\ v \end{pmatrix} = \begin{pmatrix} 1 \\ B \end{pmatrix} + \delta \left(\begin{pmatrix} (-1-i)/2 \\ 1 \end{pmatrix} C(\tilde{x}, \tilde{y}, t) e^{i\omega \tilde{t}} + c.c. + \begin{pmatrix} (-1-3i)/4 \\ 1/2 \end{pmatrix} \hat{f}_3 e^{3i\omega \tilde{t}} + c.c. \right) + O(\delta^2).$$

To obtain the equation for the complex amplitude A we extract the frequency ν_{21} and write

$$C = \sqrt{2/3} e^{i(\tan^{-1}(1/8) + \nu_{21} t)/2} A. \tag{16}$$

After rescaling the spatial coordinates as $(x, y) = \sqrt{(D_u + D_v)/2}(\tilde{x}, \tilde{y})$ we arrive at Eq.(6) with the coefficients given by

$$\begin{aligned} \mu &= b/2 + 15|\hat{f}_3|^2/8, && (17) \\ \sigma &= -(\nu_{21}/2 + 33|\hat{f}_3|^2/8), && (18) \\ \gamma &= 6\hat{f}_2/\sqrt{65}, && (19) \\ \rho &= |\hat{f}_3|\sqrt{205/24}, && (20) \\ \phi &= \tan^{-1}(14/3) + \arg(\hat{f}_3). && (21) \end{aligned}$$

As before $\nu = \nu_{22} - \nu_{21}$ and $\eta = \rho e^{i\phi}$.

To give an impression of the temporal evolution of the patterns as they may be seen in experiments we show in (SimulationOver2Periods_withFastOscs.mov) (see also Fig.18) a movie of the u-component of the Brusselator. More precisely, we show only the spatial dependence associated with the wavevectors on the critical circle. In terms of the expansion (10) the corresponding amplitudes can be written as

$$\begin{aligned} u_k = & Z \left(\left(-\frac{1}{2} - \frac{i}{2} \right) \sqrt{\frac{2}{3}} \sum_{n=-\infty}^{\infty} (X_n + iY_n) e^{in\nu t} e^{i\nu_{21} t/2 + i\omega \tilde{t}} \right. \\ & \left. + \left(-\frac{1}{2} + \frac{i}{2} \right) \sqrt{\frac{2}{3}} \sum_{n=-\infty}^{\infty} (X_n - iY_n) e^{in\nu t} e^{-i\nu_{21} t/2 - i\omega \tilde{t}} \right). \end{aligned}$$

Here Z represents the steady-state amplitude of the Fourier mode given by the fixed-point solution of Eq.11.

References

[1] B. Christiansen, P. Alstrom, and M. T. Levinsen. Ordered capillary-wave states - quasi-crystals, hexagons, and radial waves. *Phys. Rev. Lett.*, 68(14):2157–2160, April 1992.

[2] W. S. Edwards and S. Fauve. Parametrically excited quasi-crystalline surface-waves. *Phys. Rev. E*, 47(2):R788–R791, February 1993.

[3] W. S. Edwards and S. Fauve. Patterns and quasi-patterns in the Faraday experiment. *J. Fluid Mech.*, 278:123, 1994.

[4] A. Kudrolli and J.P. Gollub. Localized spatiotemporal chaos in surface waves. *Phys. Rev. E*, 54:1052, 1996.

[5] A. Kudrolli, B. Pier, and J.P. Gollub. Superlattice patterns in surface waves. *Physica D*, 123:99, 1998.

[6] H. Arbell and J. Fineberg. Two-mode rhomboidal states in driven surface waves. *Phys. Rev. Lett.*, 84(4):654–657, January 2000.

[7] H. Arbell and J. Fineberg. Pattern formation in two-frequency forced parametric waves. *Phys. Rev. E*, 65:036224, 2002.

[8] M.-T. Westra, D. J. Binks, and W. van de Water. Patterns of faraday waves. *J. Fluid Mech.*, 496:1, 2003.

[9] Y. Ding and P. Umbanhowar. Enhanced faraday pattern stability with three-frequency driving. *Phys. Rev. E*, 73:046305, 2006.

[10] R. Herrero, E. Grosse Westhoff, A. Aumann, T. Ackemann, Yu. A. Logvin, and W. Lange. Twelvefold quasiperiodic patterns in a nonlinear optical system with continuous rotational symmetry. *Phys. Rev. Lett.*, 82:4627, 1999.

[11] J. L. Rogers, W. Pesch, O. Brausch, and M. F. Schatz. Complex-ordered patterns in shaken convection. *Phys. Rev. E*, 71(6):066214, June 2005.

[12] H.-K Ko, J. Lee, and K. J. Lee. Subharmonic bifurcations of standing wave lattices in a driven ferrofluid system. *Phys. Rev. E*, 65:056222, 2002.

[13] D. Shechtman , I. Blech , D. Gratias , and J. Cahn . Metallic phase with long-range orientational order and no translational symmetry. *Phys. Rev. Lett.*, 53:1951, 1984.

[14] N. D. Mermin and S. M. Troian. Mean-field theory of quasicrystalline order. *Phys. Rev. Lett.*, 54:1524, 1985.

[15] A. C. Newell and Y. Pomeau. Turbulent crystals in macroscopic systems. *J. Phys. A*, 26(8):L429–L434, April 1993.

[16] X. B. Zeng, G. Ungar, Y. S. Liu, V. Percec, S. E. Dulcey, and J. K. Hobbs. Supramolecular dendritic liquid quasicrystals. *Nature*, 428(6979):157–160, March 2004.

[17] R. Lifshitz and H. Diamant. Soft quasicrystals - why are they stable? *Phil. Mag.*, 87(18-21):3021–3030, 2007.

[18] R. Lifshitz and D.M. Petrich. Theoretical model for Faraday waves with multiple-frequency forcing. *Phys. Rev. Lett.*, 79:1261, 1997.

[19] M. Silber, C. M. Topaz, and A. C. Skeldon. Two-frequency forced Faraday waves: Weakly damped modes and pattern selection. *Physica D*, 143(1-4):205–225, September 2000.

[20] J. Porter, C. M. Topaz, and M. Silber. Pattern control via multifrequency parametric forcing. *Phys. Rev. Lett.*, 93(3):034502, July 2004.

[21] J. Porter and M. Silber. Resonant triad dynamics in weakly damped faraday waves with two-frequency forcing. *Physica D*, 190:93–114, 2004.

[22] A. M. Rucklidge and M. Silber. Quasipatterns in parametrically forced systems. *Phys. Rev. E*, 75:055203, 2007.

[23] W. Zhang and J. Viñals. Square patterns and quasi-patterns in weakly damped Faraday waves. *Phys. Rev. E*, 53:4283, 1996.

[24] P. L. Chen and J. Viñals. Pattern selection in Faraday waves. *Phys. Rev. Lett.*, 79(14):2670–2673, October 1997.

[25] W. Zhang and J. Viñals. Pattern formation in weakly damped parametric surface waves. *J. Fluid Mech.*, 336:301, 1997.

[26] W. Zhang and J. Viñals. Pattern formation in weakly damped parametric surface waves driven by two frequency components. *J. Fluid Mech.*, 341:225, 1997.

[27] W. Zhang and J. Viñals. Numerical study of pattern formation in weakly damped parametric surface waves. *Physica D*, 116:225, 1998.

[28] P. Chen and J. Viñals. Amplitude equations and pattern selection in Faraday waves. *Phys. Rev. E*, 60:559, 1999.

[29] B. Malomed, A. A. Nepomnyashchy, and M. I. Tribelsky. Two-dimensional quasiperiodic structures in nonequilibrium systems. *Sov. Phys. JETP*, 69:388, 1989.

[30] H. Chaté and P. Manneville. Phase diagram of the two-dimensional complex Ginzburg-Landau equation. *Physica A*, 224:348, 1996.

[31] Q. Ouyang and J. M. Flesselles. Transition from spirals to defect turbulence driven by a convective instability. *Nature*, 379(6561):143–146, January 1996.

[32] A. L. Belmonte, Qi Ouyang, and J. M. Flesselles. Experimental survey of spiral dynamics in the belousov-zhabotinsky reaction. *J. Phys. II (Paris)*, 7(10):1425–1468, October 1997.

[33] I. S. Aranson and L. Kramer. The world of the complex Ginzburg-Landau equation. *Rev. Mod. Phys.*, 74:99, 2002.

[34] S. Madruga, H. Riecke, and W. Pesch. Defect chaos and bursts: Hexagonal rotating convection and the Complex Ginzburg-Landau equation. *Phys. Rev. Lett.*, 96:074501, 2006.

[35] P. Coullet and K. Emilsson. Strong resonances of spatially distributed oscillators: a laboratory to study patterns and defects. *Physica D*, 61:119, 1992.

[36] P. Coullet, T. Frisch, and G. Sonnino. Dispersion-induced patterns. *Phys. Rev. E*, 49:2087, 1994.

[37] V. Petrov, Q. Ouyang, and H. L. Swinney. Resonant pattern formation in a chemical system. *Nature*, 388(6643):655–657, August 1997.

[38] A. L. Lin, M. Bertram, K. Martinez, H. L. Swinney, A. Ardelea, and G. F. Carey. Resonant phase patterns in a reaction-diffusion system. *Phys. Rev. Lett.*, 84(18):4240–4243, May 2000.

[39] A. L. Lin, A. Hagberg, A. Ardelea, M. Bertram, H. L. Swinney, and E. Meron. Four-phase patterns in forced oscillatory systems. *Phys. Rev. E*, 62(3):3790–3798, September 2000.

[40] A.L. Lin, A. Hagberg, E. Meron, and H.L. Swinney. Resonance tongues and patterns in periodically forced reaction-diffusion systems. *Phys. Rev. E.*, 69:066217, 2004.

[41] M. Dolnik, I. Berenstein, A. M. Zhabotinsky, and I. R. Epstein. Spatial periodic forcing of Turing structures. *Phys. Rev. Lett.*, 87(23):238301, December 2001.

[42] I. Berenstein, L. Yang, M. Dolnik, A. M. Zhabotinsky, and I. Epstein. Superlattice Turing structures in a photosensitive reaction-diffusion system. *Phys. Rev. Lett.*, 91(5):058302, August 2003.

[43] J .M Conway and H. Riecke. Quasi-patterns in a model of chemical oscillations with multi-resonant forcing. *Phys. Rev. Lett.*, 99:218301, 2007.

[44] H. Riecke, J. D. Crawford, and E. Knobloch. Time-modulated oscillatory convection. *Phys. Rev. Lett.*, 61:1942, 1988.

[45] J. M. Conway and H. Riecke. Pattern selection in the complex Ginzburg-Landau equation with multi-resonant forcing. *Phys. Rev. E*, 76:057202, 2007.

[46] K. Kumar and L. S. Tuckerman. Parametric instability of the interface between two fluids. *J. Fluid Mech.*, 279:49, 1994.

[47] A. M. Rucklidge and W. J. Rucklidge. Convergence properties of the 8, 10, and 12 mode representations of quasipatterns. *Physica D*, 178:62, 2003.

[48] F. Hynne and P. G. Sørensen. Experimental determination of Ginzburg-Landau parameters for reaction-diffusion systems. *Phys. Rev. E*, 48:4106–4109, 1993.

[49] Y. Pomeau. Front motion, metastability and subcritical bifurcations in hydrodynamics. *Physica D*, 23:3, 1986.

[50] D. Boyer and J. Viñals. Grain boundary pinning and glassy dynamics in stripe phases. *Phys. Rev. E*, 65(4):046119, April 2002.

[51] H. W. Müller. Periodic triangular patterns in the Faraday experiment. *Phys. Rev. Lett.*, 71:3287, 1993.

[52] B. Dionne, M. Silber, and A. C. Skeldon. Stability results for steady, spatially periodic planforms. *Nonlinearity*, 10(2):321–353, March 1997.

[53] J. Porter, C. M. Topaz, and M. Silber. Faraday wave pattern selection via multi-frequency forcing. *Phys. Rev. Lett.*, 93:034502, 2004.

[54] A. Yochelis, A. Hagberg, E. Meron, A. L. Lin, and H. L. Swinney. Development of standing-wave labyrinthine patterns. *SIAM J. Appl. Dyn. Systems*, 1:236, 2002.

[55] H. Riecke and S. Madruga. Geometric diagnostics of complex patterns: Spiral-defect chaos. *Chaos*, 16:013125, 2006.

[56] C. Harrison, D. H. Adamson, Z. D. Cheng, J. M. Sebastian, S. Sethuraman, D. A. Huse, R. A. Register, and P. M. Chaikin. Mechanisms of ordering in striped patterns. *Science*, 290:1558–1560, 2000.

[57] D. Boyer and J. Viñals. Domain coarsening of stripe patterns close to onset. *Phys. Rev. E*, 6405(5):050101, November 2001.

[58] C. Sagui and R. C. Desai. Late-stage kinetics of systems with competing interactions quenched into the hexagonal phase. *Phys. Rev. E*, 52(3):2807–2821, September 1995.

[59] B. Echebarria and H. Riecke. Sideband instabilities and defects of quasipatterns. *Physica D*, 158:45, 2001.